Joint Symbol-Level Precoding and Reflecting Designs for RIS-Enhanced MU-MISO Systems

Rang Liu, *Student Member, IEEE,* Ming Li, *Senior Member, IEEE,* Qian Liu, *Member, IEEE,* and A. Lee Swindlehurst, *Fellow, IEEE*

Abstract

Reconfigurable intelligent surfaces (RIS) have emerged as a revolutionary solution to enhance wireless communications by changing propagation environment in a cost-effective and hardware-efficient fashion. In addition, symbol-level precoding (SLP) technique has attracted considerable attention recently due to its advantages in converting multiuser interference (MUI) into useful signals. Therefore, it is of interest to investigate the employment of RIS in symbol-level precoding systems to exploit MUI in a more effective way by manipulating the multiuser channels. In this paper, we focus on joint symbol-level precoding and reflecting designs in RIS-enhanced multiuser multiple-input single-output (MU-MISO) systems. Both power minimization and quality-of-service (QoS) balancing problems are considered. In order to solve the joint optimization problems, we develop an efficient iterative algorithm to decompose them into separate symbol-level precoding and block-level reflecting design problems. An efficient gradient-projection-based algorithm is utilized to design the symbol-level precoding and a Riemannian conjugate gradient (RCG)-based algorithm is employed to solve the reflecting design problem. Simulation results demonstrate the significant performance improvement introduced by the RIS and illustrate the effectiveness of our proposed algorithms.

Index Terms

Reconfigurable intelligent surface (RIS), symbol-level precoding (SLP), multiuser multiple-input single-output (MU-MISO) systems, manifold optimization.

R. Liu and M. Li are with the School of Information and Communication Engineering, Dalian University of Technology, Dalian 116024, China (e-mail: liurang@mail.dlut.edu.cn; mli@dlut.edu.cn).

Q. Liu is with the School of Computer Science and Technology, Dalian University of Technology, Dalian 116024, China (e-mail: qianliu@dlut.edu.cn).

A. L. Swindlehurst is with the center for Pervasive Communications and Computing, University of California, Irvine, CA 92697, USA (e-mail: swindle@uci.edu).

I. Introduction

During the past decade, the applications of wireless communications have been growing rapidly and now affect nearly every aspect of our daily life. Meanwhile, the demands of wireless communication networks for high data rate and low latency are also continuously increasing. Various technical solutions have been proposed to meet the requirements of fifth-generation (5G) networks and beyond. Among those technologies, massive multi-input multi-output (MIMO), millimeter wave (mmWave) communications, and ultra-dense networks are deemed as three fundamental approaches to enhance the performance along three basic dimensions: Improving spectral efficiency, utilizing more spectrum, and exploiting spatial reuse [1], [2]. However, it seems that the performance improvements offered by these approaches are reaching their limits, and new technologies in different directions are needed to achieve further fundamental advances in wireless networks. One such technology is the use of reconfigurable intelligent surface (RIS), which is a potentially revolutionary approach that provides additional degrees of freedom in system design by intelligently changing the propagation environment [3]-[6].

RIS is a planar array composed of a large number of reconfigurable passive reflecting elements, e.g., phase shifters, that can independently introduce certain phase shifts to the incident electromagnetic (EM) waves. Thus, RIS can intelligently manipulate EM waves by properly adjusting their reflection coefficients to produce a favorable propagation environment, especially when faced with blockages or severe fading. New research on micro-electrical-mechanical systems (MEMS) and meta-materials has enabled the RIS to be configured in real-time, which is necessary for the rapidly changing wireless communication environment. RIS have the potential for greatly expanding coverage, improving transmission quality, and enhancing security, etc., in a cost-effective and hardware-efficient fashion. Moreover, these lightweight devices can be easily attached to the surfaces of buildings or some mobile equipment, which provides mobility and portability for practical implementation [4], [5].

Attracted by above advantages, researchers have devoted considerable attention to the development of RIS in recent months. The applications of RIS to different systems have been investigated to enhance their performance with different performance goals [7]-[24]. By properly designing the phase-shifting components of the RIS, the reflected signals can be coherently added to the received signals from other

paths at intended receivers, which facilitates minimization of the transmit power [7]-[11], or improving transmission performance in terms of spectral efficiency [12], quality of service [7], [13], energy reception [14], ergodic capacity [15], symbol error rate [16], channel capacity [17], received signal power [18], sum-rate [19], [20], and enhancing the power efficiency [21], etc. RIS-enhanced physical layer security has also been investigated in [22]-[24]. In [25], the authors show that an RIS-enhanced system exhibits better rate and energy efficiency performance than a conventional decode-and-forward relay system when the RIS is relatively large. An analysis of the impact of phase errors in RIS systems was provided in [26], and free-space path loss models for RIS-enhanced wireless communications was studied in [27], [28].

Precoding design is also of significant importance to facilitate information transmissions in RIS-enhanced multi-user systems. In existing works, multi-user interference (MUI) is regarded as a harmful component and suppressed by the precoding and reflecting designs as much as possible. However, recent research [29]-[32] has found that MUI can often be treated as a useful signal to enhance information transmissions by means of symbol-level precoding techniques. Specifically, symbol-level precoding utilizes transmitted symbol information and channel state information (CSI) to design the precoder, which converts harmful MUI into constructive interference to improve the symbol detection performance compared with block-level precoding.

Motivated by these findings, we propose to combine symbol-level precoding and RIS in order to enjoy the advantages of both technologies. The employment of RIS can facilitate the exploitation of MUI in symbol-level precoding by favorably manipulating the multi-user propagation channels. However, there are some obstacles that must be tackled. First, the symbol-level precoder changes with each transmitted symbol vector, while the RIS reflects all of them with the same phase-shift beamforming. Thus, symbol-level constraints are difficult to implement in the reflecting design. Since both the symbol-level precoding and reflecting need to consider all possible transmit vectors, the computational complexity will be tremendously high for large-scale systems and high-level modulation types. To the best of our knowledge, this problem has not been studied yet, which motivates the work in this paper.

We consider the joint design of symbol-level precoding and RIS transmission design in multi-user multi-input single-output (MU-MISO) systems. In particular, we consider a multi-antenna base station

(BS) serving a number of single-antenna users with the aid of an RIS, which consists of many reflecting elements. We aim to design the symbol-level precoding and RIS reflection to enhance the system performance by exploiting both MUI and modifications to the propagation environment. The main contributions in this paper are summarized as follows:

- We investigate, for the first time, the joint design of symbol-level precoding and RIS transmission in MU-MISO systems.
- We first aim to minimize the average transmit power as well as guarantee a certain quality-of-service (QoS) for the information transmissions. In order to solve this joint design problem, an efficient iterative algorithm is proposed to decompose the problem into separate symbol-level precoding and reflecting designs, where the gradient-projection-based and Riemannian conjugate gradient (RCG)-based algorithms are exploited.
- Then, with a given average transmit power constraint, we investigate the QoS balancing problem, where the symbol-level precoding and reflecting are iteratively updated using similar gradient-projection-based and RCG-based algorithms after some transformations.
- Finally, we provide extensive simulation results to demonstrate the advantages of applying RIS in symbol-level precoding MU-MISO systems and the effectiveness of our proposed algorithms.

The rest of this paper is organized as follows. Section II introduces the system model of our proposed RIS-enhanced MU-MISO system. The considered power minimization and QoS balancing problems are investigated in Sections III and IV, respectively. The algorithm initialization and complexity analysis are presented in Section V. Simulation results are presented in Section VI, and finally conclusions are provided in Section VII.

The following notation is used throughout this paper. Boldface lower-case and upper-case letters indicate column vectors and matrices, respectively. $(\cdot)^T$, and $(\cdot)^H$ denote the transpose and the transpose-conjugate operations, respectively. $\mathbb{C}$ denotes the set of complex numbers. $|a|$ and $\|\mathbf{a}\|$ are the magnitude of a scalar a and the norm of a vector $\mathbf{a}$, respectively. $\angle a$ is the angle of complex-valued a. $\Re\{\cdot\}$ and $\Im\{\cdot\}$ denote the real and imaginary part of a complex number, respectively. $\mathrm{diag}\{\mathbf{a}\}$ indicates the diagonal matrix whose diagonals are the elements of $\mathbf{a}$. $\mathbf{A} \succeq \mathbf{0}$ indicates that the matrix $\mathbf{A}$ is positive semi-definite. Finally, we

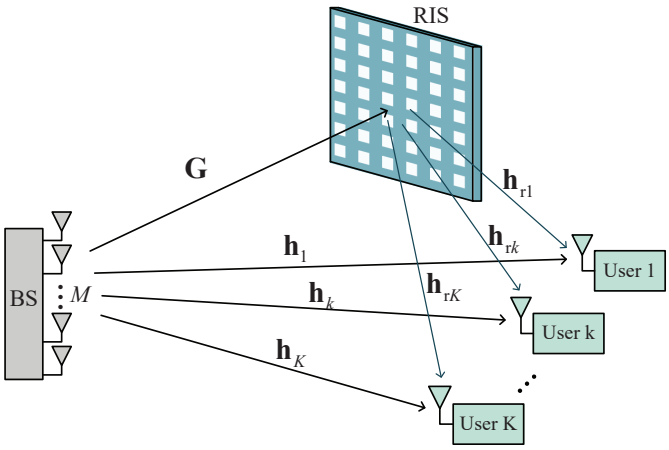

Fig. 1: The RIS-enhanced MU-MISO system.

adopt the following indexing notation: $\mathbf{A}(i,j)$ denotes the element of the i-th row and the j-th column of matrix $\mathbf{A}$, $\mathbf{a}(i)$ denotes the i-th element of vector $\mathbf{a}$.

II. System Model

We consider an RIS-enhanced MU-MISO system as shown in Fig. 1, where a BS equipped with M antennas serves K single-antenna users with the aid of an RIS. The RIS consists of N passive reflecting elements, which are implemented by phase shifters and denoted as $\boldsymbol{\theta} \triangleq [\theta_1, \ldots, \theta_N]$ that satisfy $|\theta_n| = 1, \forall n$. We denote $\mathbf{G} \in \mathbb{C}^{N\times M}$, $\mathbf{h}_k \in \mathbb{C}^{M\times 1}$, and $\mathbf{h}_{rk} \in \mathbb{C}^{N\times 1}$ as the channels from BS to RIS, from BS to the k-th user and from RIS to the k-th user, respectively. In this paper, we assume that the channel state information (CSI) of all channels is known perfectly and instantaneously to the BS[1].

To facilitate the symbol-level precoding technique, we assume the transmitted symbols are independently selected from a Ω-phase shift keying (PSK) constellation[2] (i.e., $\Omega = 2, 4, \ldots$). Therefore, the transmitted symbol vector $\mathbf{s}_m \triangleq [s_{m,1}, \ldots, s_{m,K}]$ has Ω^K combinations, i.e., $m = 1, \ldots, \Omega^K$. For different $\mathbf{s}_m$, the BS changes its transmitted precoder vector $\mathbf{x}_m \in \mathbb{C}^{M\times 1}$ in order to exploit the MUI. Unlike conventional block-level precoding techniques, the mapping from $\mathbf{s}_m$ to $\mathbf{x}_m$ is usually nonlinear.

Through the direct and reflected paths, the compound received signal at the k-th user can be written as

$$r_{m,k} = \left(\mathbf{h}_k^H + \mathbf{h}_{rk}^H \boldsymbol{\Theta} \mathbf{G}\right) \mathbf{x}_m + n_k, \forall m, \tag{1}$$

[1]Channel estimation for RIS-enhanced systems has been studied in [33]-[35].

[2]We should emphasize that symbol-level precoding is related to the modulation type. Therefore, our designs in this paper are only capable of exploiting PSK modulation. The design for QAM modulation will be investigated in future work.

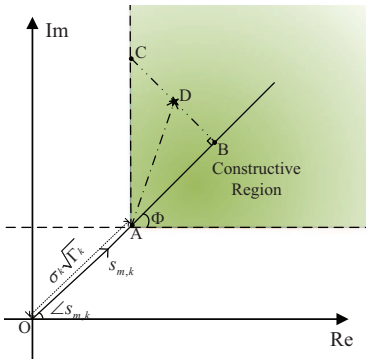

(a) An example of the constructive region.

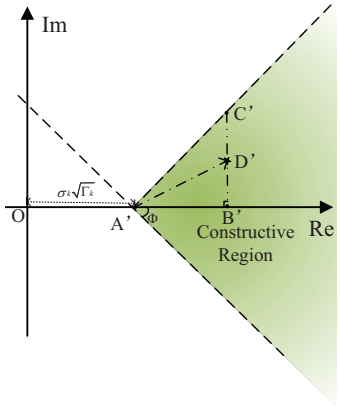

(b) After rotating the diagram in Fig. 2(a) clockwise by $\angle s_{m,k}$ degrees.

Fig. 2: Constructive region for QPSK symbols.

where $\mathbf{\Theta} \triangleq \mathrm{diag}\left\{\boldsymbol{\theta}\right\}$ denotes the phase shifts of the RIS, and $n_k \sim \mathcal{CN}(0, \sigma_k^2)$ is additive white Gaussian noise (AWGN) for the k-th user. Moreover, it is noteworthy that, during a coherent time slot with the same CSI, the BS changes $\mathbf{x}_m$ according to the transmitted symbols while the RIS phase shifts $\boldsymbol{\theta}$ remains unchanged. Therefore, the reflecting design should consider all possible Ω^K precoding vectors. Defining the precoding matrix $\mathbf{X} \triangleq [\mathbf{x}_1, \ldots, \mathbf{x}_{\Omega^K}]$, the average transmit power required to send a given symbol vector is

$$P_{\text{ave}} = \frac{\|\mathbf{X}\|_F^2}{\Omega^K}. \tag{2}$$

With knowledge of symbols to be transmitted, symbol-level precoding makes the MUI constructive to the information transmissions by elaborately designing $\mathbf{x}_m$. In particular, the MUI is converted into constructive interference if it can push the received signals away from the PSK decision boundaries. In order to illustrate the idea behind constructive interference, without loss of generality, we take quadrature

phase shift keying (QPSK) as an example ($\Omega = 4$). For simplicity, we also consider $\left(\frac{1}{\sqrt{2}}, \frac{1}{\sqrt{2}}j\right)$ as the symbol of interest for the k-th user and show the received signal in the complex plane as in Fig. 2(a). Since the decision boundaries for this symbol of interest are the positive halves of the x and y axes, as long as the noise-corrupted received signal expressed in (1) is in the first quadrant, the receiver can correctly detect the desired signal. However, when we design the precoder $\mathbf{x}_m$, the noise is unknown and cannot be predicted beforehand.

Denote the received noise-free signal of the k-th user as

$$\widetilde{r}_{m,k} = \left(\mathbf{h}_k^H + \mathbf{h}_{\mathrm{r}k}^H \boldsymbol{\Theta} \mathbf{G}\right) \mathbf{x}_m, \tag{3}$$

which is illustrated as point D in Fig. 2(a). To reduce the impact of noise on the symbol detection, it is desirable to design $\mathbf{x}_m$ such that point D is sufficiently far away from the corresponding decision boundaries to satisfy the QoS. In order to quantify the QoS requirement, let Γ_k be the SNR requirement for the k-th user. If we ignore the impact of MUI and focus on the single-user case, the received noise-free signal should be at point A to ensure that $\frac{|\widetilde{r}_{m,k}|^2}{\sigma_k^2} = \Gamma_k$, i.e., $\overrightarrow{OA} = \sigma_k \sqrt{\Gamma_k} \mathbf{s}_m(k)$. Considering the multi-user signal as in (1), symbol-level precoding aims to design $\mathbf{x}_m$ such that point D lies in the constructive (green) region, where the distance between received signal and its decision boundaries, which can be expressed as $\sigma_k \sqrt{\Gamma_k} \cos \Phi$, is guaranteed to satisfy the SNR requirement. Therefore, symbol-level precoding can achieve better SER performance by converting the MUI into a constructive component.

In order to geometrically express this relationship, we project point D on the direction of $\overrightarrow{OA}$ at point B, and we define point C to be the intersection of the extension of $\overrightarrow{BD}$ and the boundaries of the constructive region. Then, the received noise-free signal in the green region should satisfy

$$\left|\overrightarrow{BC}\right| - \left|\overrightarrow{BD}\right| \geq 0. \tag{4}$$

To make this expression clearer, we rotate the diagram in Fig. 2(a) clockwise by $\angle s_{m,k}$ degrees as shown in Fig. 2(b). Then, the QoS requirement is readily expressed as

$$\left[\Re\left\{\widetilde{r}_{m,k} e^{-j\angle s_{m,k}}\right\} - \sigma_k \sqrt{\Gamma_k}\right] \tan \Phi - \left|\Im\left\{\widetilde{r}_{m,k} e^{-j\angle s_{m,k}}\right\}\right| \geq 0, \forall k, \forall m. \tag{5}$$

In this paper, we consider two typical optimization problems for RIS-enhanced MU-MISO systems: *i*) the power minimization problem, which minimizes the average transmit power while guaranteeing the QoS of the data received by the users; *ii*) the QoS balancing problem, which aims to maximize the minimum QoS with a given average transmit power budget. In the following sections, we will formulate and solve these two problems.

III. Algorithm for Power Minimization Problem

With the previous analysis, the average power minimization problem can be written as

$$\min_{\mathbf{X},\boldsymbol{\theta}} \quad \|\mathbf{X}\|_F^2 \tag{6a}$$

$$\text{s.t.} \quad \left[\Re\left\{\widetilde{r}_{m,k}e^{-j\angle s_{m,k}}\right\} - \sigma_k\sqrt{\Gamma_k}\right]\tan\Phi - \left|\Im\left\{\widetilde{r}_{m,k}e^{-j\angle s_{m,k}}\right\}\right| \geq 0, \forall k, \forall m, \tag{6b}$$

$$\widetilde{r}_{m,k} = \left(\mathbf{h}_k^H + \mathbf{h}_{\mathrm{r}k}^H\boldsymbol{\Theta}\mathbf{G}\right)\mathbf{x}_m, \forall k, \forall m, \tag{6c}$$

$$\boldsymbol{\Theta} = \mathrm{diag}\{\boldsymbol{\theta}\}, |\theta_n| = 1, \forall n, \tag{6d}$$

which is non-convex due to the RIS constraints (6d). Furthermore, the size of $\mathbf{X} \in \mathbb{C}^{M\times\Omega^K}$ is huge even for the relatively small K and Ω. Thus, it is difficult to directly solve this large-scale joint symbol-level precoding and reflecting problem. In order to tackle this difficulty, we propose to decompose the bivariate problem into two sub-problems and implement the solutions iteratively.

A. Symbol-Level Precoding Design for Power Minimization Problem

When the RIS phase shifts $\boldsymbol{\theta}$ are fixed, the overall channel vector is determined. We denote the combined channel vector from BS to the k-th user as $\widetilde{\mathbf{h}}_k^H \triangleq \mathbf{h}_k^H + \mathbf{h}_{\mathrm{r}k}^H\boldsymbol{\Theta}\mathbf{G}, \forall k$. Since the precoder vectors $\mathbf{x}_m, m = 1, \ldots, \Omega^K$, are independent of each other, the power minimization problem (6) can be divided into Ω^K sub-problems. The m-th sub-problem for optimizing $\mathbf{x}_m$ is given by

$$\min_{\mathbf{x}_m} \quad \|\mathbf{x}_m\|^2 \tag{7a}$$

$$\text{s.t.} \quad \left[\Re\left\{\widetilde{\mathbf{h}}_k^H\mathbf{x}_m e^{-j\angle s_{m,k}}\right\} - \sigma_k\sqrt{\Gamma_k}\right]\tan\Phi - \left|\Im\left\{\widetilde{\mathbf{h}}_k^H\mathbf{x}_m e^{-j\angle s_{m,k}}\right\}\right| \geq 0, \forall k. \tag{7b}$$

This is a convex optimization problem and can be solved by standard convex tools, e.g. the CVX solver [36]. In addition, an efficient gradient projection algorithm with low complexity has also been studied in

[30], where this problem was first converted into a real-valued format, then its Lagrangian dual function was derived to facilitate the gradient projection algorithm. Due to space limitations, details of the algorithm to solve (7) are omitted.

B. Reflecting Design for Power Minimization Problem

After obtaining the precoder vectors $\mathbf{x}_m, m = 1, \ldots, \Omega^K$, the objective of the original optimization problem (6) has been determined. This means that, with given $\mathbf{x}_m$, the reflecting design of $\boldsymbol{\theta}$ could not directly affect the power minimization objective of (6). Therefore, for the reflecting design, we attempt to formulate another proper objective function that enhances the reduction of the transmit power for future iterations.

Since the power minimization problem (7) is convex, the optimal $\mathbf{x}_m$ usually makes the left-hand side of constraint (7b) equal to a relatively small positive value, i.e., the QoS requirement is satisfied almost with equality. In order to further reduce the transmit power in the next iteration, we propose to design the RIS phase shifts $\boldsymbol{\theta}$ using the stricter constraint (8b) in place of (7b), which can introduce an improved QoS that can provide more freedom for power minimization in the next iteration. To this end, the RIS reflecting design problem is transformed to

$$\max_{\boldsymbol{\theta}, \alpha_{m,k}} \quad \sum_{m=1}^{\Omega^K} \sum_{k=1}^{K} \alpha_{m,k} \tag{8a}$$

$$\text{s.t.} \quad \left[\Re\left\{\widetilde{r}_{m,k} e^{-j\angle s_{m,k}}\right\} - \sigma_k \sqrt{\Gamma_k}\right] \tan\Phi - \left|\Im\left\{\widetilde{r}_{m,k} e^{-j\angle s_{m,k}}\right\}\right| \geq \alpha_{m,k}, \forall k, \forall m, \tag{8b}$$

$$\widetilde{r}_{m,k} = \left(\mathbf{h}_k^H + \mathbf{h}_{\mathrm{r}k}^H \boldsymbol{\Theta} \mathbf{G}\right) \mathbf{x}_m, \forall k, \forall m, \tag{8c}$$

$$\boldsymbol{\Theta} = \mathrm{diag}\{\boldsymbol{\theta}\}, |\theta_n| = 1, \forall n, \tag{8d}$$

where the auxiliary variable $\alpha_{m,k}$ can be viewed as the residual QoS requirement. Then, by defining

$$a_{m,k} \triangleq \mathbf{h}_k^H \mathbf{x}_m e^{-j\angle s_{m,k}}, \forall k, \forall m, \tag{9a}$$

$$\mathbf{b}_{m,k} \triangleq \mathrm{diag}\left\{\mathbf{h}_{\mathrm{r}k}^H\right\} \mathbf{G} \mathbf{x}_m e^{-j\angle s_{m,k}}, \forall k, \forall m, \tag{9b}$$

$$\widehat{r}_{m,k} \triangleq a_{m,k} + \boldsymbol{\theta}^H \mathbf{b}_{m,k}, \tag{9c}$$

problem (8) can be reformulated concisely as

$$\min_{\boldsymbol{\theta}} \sum_{m=1}^{\Omega^K} \sum_{k=1}^{K} \left|\Im\left\{\widehat{r}_{m,k}\right\}\right| - \left[\Re\left\{\widehat{r}_{m,k}\right\} - \sigma_k\sqrt{\Gamma_k}\right] \tan\Phi \tag{10a}$$

$$\text{s.t. } |\theta_n| = 1, \forall n. \tag{10b}$$

Unfortunately, the absolute values in the objective (10a) are non-differentiable, which hinders the algorithm development. In addition, the unit modulus constraints for the RIS phase shifts in (10b) introduce another difficulty due to their non-convexity. Thus, we turn to solve above two problems by the log-sum-exp and manifold-based algorithms in the followings.

In order to handle the absolute value terms, we attempt to convert the objective (10a) into a differentiable function. It can be observed that (10a) can be concisely expressed as $|a| + b$, where a and b are scalars. Then, the non-differentiable absolute value function can be replaced by

$$|a| + b = \max\left\{a + b, -a + b\right\}. \tag{11}$$

We then exploit the well-known log-sum-exp method and obtain

$$\max\left\{a + b, -a + b\right\} \approx \varepsilon \log\left[\exp\left(\frac{a+b}{\varepsilon}\right) + \exp\left(\frac{-a+b}{\varepsilon}\right)\right], \tag{12}$$

where ε is a relatively small positive number to maintain the approximation. Thus, the optimization problem (10) can be reformulated as

$$\min_{\boldsymbol{\theta}} \quad g \triangleq \sum_{i=1}^{K\Omega^K} \varepsilon \log\left[\exp\left(\frac{f_{2i-1}}{\varepsilon}\right) + \exp\left(\frac{f_{2i}}{\varepsilon}\right)\right] \tag{13a}$$

$$\text{s.t.} \qquad |\theta_n| = 1, \forall n. \tag{13b}$$

For simplicity, in (13) we define $f_i, i = 1, 2, \ldots, 2K\Omega^K$, as

$$f_{2i-1} \triangleq \Im\left\{\widehat{r}_{m,k}\right\} - \left[\Re\left\{\widehat{r}_{m,k}\right\} - \sigma_k\sqrt{\Gamma_k}\right] \tan\Phi = \Re\{\boldsymbol{\theta}^H\}\mathbf{a}_{2i-1} + \Im\{\boldsymbol{\theta}^H\}\mathbf{b}_{2i-1} + c_{2i-1}, \tag{14a}$$

$$f_{2i} \quad \triangleq -\Im\left\{\widehat{r}_{m,k}\right\} - \left[\Re\left\{\widehat{r}_{m,k}\right\} - \sigma_k\sqrt{\Gamma_k}\right] \tan\Phi = \Re\{\boldsymbol{\theta}^H\}\mathbf{a}_{2i} + \Im\{\boldsymbol{\theta}^H\}\mathbf{b}_{2i} + c_{2i}, \tag{14b}$$

where $i = K(m-1)+k$ and

$$\mathbf{a}_{2i-1} \triangleq \Im\{\mathbf{b}_{m,k}\} - \Re\{\mathbf{b}_{m,k}\}\tan\Phi, \tag{15a}$$

$$\mathbf{b}_{2i-1} \triangleq \Re\{\mathbf{b}_{m,k}\} + \Im\{\mathbf{b}_{m,k}\}\tan\Phi, \tag{15b}$$

$$c_{2i-1} \triangleq \Im\{a_{m,k}\} - \Re\{a_{m,k}\}\tan\Phi + \sigma_k\sqrt{\Gamma_k}\tan\Phi, \tag{15c}$$

$$\mathbf{a}_{2i} \triangleq -\Im\{\mathbf{b}_{m,k}\} - \Re\{\mathbf{b}_{m,k}\}\tan\Phi, \tag{15d}$$

$$\mathbf{b}_{2i} \triangleq -\Re\{\mathbf{b}_{m,k}\} + \Im\{\mathbf{b}_{m,k}\}\tan\Phi, \tag{15e}$$

$$c_{2i} \triangleq -\Im\{a_{m,k}\} - \Re\{a_{m,k}\}\tan\Phi + \sigma_k\sqrt{\Gamma_k}\tan\Phi. \tag{15f}$$

While the objective of (13) is smooth and differentiable, the unit modulus constraints (13b) are non-convex, which still makes the problem difficult to solve. Two popular methods for handling this type of constraint include non-convex relaxation and alternating minimization. However, the non-convex relaxation method always suffers a performance loss since the solution is based on a relaxation of the original problem. On the other hand, the alternating minimization method may have slow convergence due to the large number of variables involved. In order to deal with these difficulties, we adopt the Riemannian-manifold-based algorithm, which can achieve a locally optimal solution of the original optimization problem with very fast convergence [37].

Before the algorithm development, we need to introduce some related concepts. On a manifold, each point has a neighborhood homeomorphic to Euclidean space, and the directions in which the point can move are its tangent vectors, which compose the tangent space. Similar to the Euclidean space, the tangent space has one tangent vector in the direction where the objective function decreases fastest, which is referred to as the Riemannian gradient. Furthermore, the Riemannian gradient is the orthogonal projection of the Euclidean gradient onto its corresponding tangent space. Therefore, efficient algorithms used in Euclidean space, e.g., the conjugate gradient (CG) and the trust-region methods, are suitable on the Riemannian manifold after several operations. In the following, we apply the conjugate gradient algorithm on the Riemannian manifold to solve our problem.

Denoting $\widetilde{\boldsymbol{\Theta}} \triangleq [\Re\{\boldsymbol{\theta}\}, \Im\{\boldsymbol{\theta}\}]^T$, the unit modulus constraints (13b) form a $2N$-dimensional smooth Riemannian manifold

$$\mathcal{M}=\left\{\widetilde{\mathbf{\Theta}}\in\mathbb{R}^{2\times N}:[\widetilde{\mathbf{\Theta}}(:,n)]^{T}\widetilde{\mathbf{\Theta}}(:,n)=1,\forall n\right\}, \tag{16}$$

whose tangent space is

$$T_{\widetilde{\mathbf{\Theta}}}\mathcal{M}=\left\{\mathbf{P}\in\mathbb{C}^{2\times N}:[\widetilde{\mathbf{\Theta}}(:,n)]^{T}\mathbf{P}(:,n)=0,\forall n\right\}. \tag{17}$$

In order to facilitate the conjugate gradient algorithm, the Euclidean gradient is required to determine the corresponding Riemannian gradient. Let $\widetilde{\boldsymbol{\theta}}_n$ be the n-th column of $\widetilde{\mathbf{\Theta}}$, so that the Euclidean gradient of $g(\widetilde{\mathbf{\Theta}})$ can be expressed as

$$\nabla_{\widetilde{\mathbf{\Theta}}}g=\left[\frac{\partial g}{\partial\widetilde{\boldsymbol{\theta}}_1},\ldots,\frac{\partial g}{\partial\widetilde{\boldsymbol{\theta}}_N}\right]. \tag{18}$$

Following the chain rule, the n-th column of the Euclidean gradient is calculated as

$$\frac{\partial g}{\partial\widetilde{\boldsymbol{\theta}}_n}=\frac{\partial\Re\{\boldsymbol{\theta}^H\}}{\partial\widetilde{\boldsymbol{\theta}}_n}\left(\frac{\partial g}{\partial\Re\{\boldsymbol{\theta}^H\}}\right)^{T}+\frac{\partial\Im\{\boldsymbol{\theta}^H\}}{\partial\widetilde{\boldsymbol{\theta}}_n}\left(\frac{\partial g}{\partial\Im\{\boldsymbol{\theta}^H\}}\right)^{T}. \tag{19}$$

According to the previous definition, it is obvious that

$$\frac{\partial\Re\{\boldsymbol{\theta}^H\}}{\partial\widetilde{\boldsymbol{\theta}}_n}=[\mathbf{e}_n,\mathbf{0}]^{T},\frac{\partial\Im\{\boldsymbol{\theta}^H\}}{\partial\widetilde{\boldsymbol{\theta}}_n}=[\mathbf{0},\mathbf{e}_n]^{T}, \tag{20}$$

where $\mathbf{e}_n\in\mathbb{R}^{N\times 1}$ is defined by $\mathbf{e}_n(n)=1,\mathbf{e}_n(i)=0,\forall i\neq n$. Based on (13a) and (14), we have

$$\frac{\partial g}{\partial\Re\{\boldsymbol{\theta}^H\}}=\sum_{i=1}^{K\Omega^K}\frac{\exp(f_{2i-1}/\varepsilon)\mathbf{a}_{2i-1}^{T}+\exp(f_{2i}/\varepsilon)\mathbf{a}_{2i}^{T}}{\exp(f_{2i-1}/\varepsilon)+\exp(f_{2i}/\varepsilon)}, \tag{21a}$$

$$\frac{\partial g}{\partial\Im\{\boldsymbol{\theta}^H\}}=\sum_{i=1}^{K\Omega^K}\frac{\exp(f_{2i-1}/\varepsilon)\mathbf{b}_{2i-1}^{T}+\exp(f_{2i}/\varepsilon)\mathbf{b}_{2i}^{T}}{\exp(f_{2i-1}/\varepsilon)+\exp(f_{2i}/\varepsilon)}. \tag{21b}$$

Then, the Euclidean gradient can be readily calculated by substituting (20) and (21) into (19). The Riemannian gradient is thus given by

$$\mathrm{grad}_{\widetilde{\mathbf{\Theta}}}g=\mathcal{P}_{\widetilde{\mathbf{\Theta}}}\left(\nabla_{\widetilde{\mathbf{\Theta}}}g\right)=\nabla_{\widetilde{\mathbf{\Theta}}}g-\widetilde{\mathbf{\Theta}}\mathrm{diag}\left\{\widetilde{\mathbf{\Theta}}^{T}\nabla_{\widetilde{\mathbf{\Theta}}}g\right\}, \tag{22}$$

where $\mathcal{P}_{\widetilde{\mathbf{\Theta}}}(\cdot)$ denotes the projection onto the tangent space.

With the Riemannian gradient, the conjugate gradient algorithm can be employed onto Rienmannian space, and is referred to as the Riemannian conjugate gradient (RCG) algorithm. Considering the char-

Algorithm 1 RCG-based RIS Reflecting Design

Input: $g(\widetilde{\mathbf{\Theta}})$, $\widetilde{\mathbf{\Theta}}_0 \in \mathcal{M}$, $N_{\max}$, δ_{th}.
Output: $\boldsymbol{\theta}^*$.

```
Initialize p = 0, δ = ∞, d_0 = −grad_Θ̃ g(Θ̃_0).
while p ≤ N_max and δ ≥ δ_th do
    Calculate Riemannian gradient grad_Θ̃ g(Θ̃_p) by (22).
    Choose Polak-Ribiere parameter β_p [38].
    Calculate search direction d_p by (23).
    Calculate Armijo backtracking line search step size α_p [38].
    Obtain Θ̃_p by (24).
    δ = ‖grad_Θ̃ g(Θ̃_p)‖^2
    p = p + 1.
end while
Θ̃* = Θ̃_p.
Construct θ* by (25)
```

acteristics of the Riemannian space, this line search method works in a different way than the standard CG algorithm. In the p-th iteration of RCG, the search direction $\mathbf{d}_p$ is determined by the Riemannian gradient $\text{grad}_{\widetilde{\mathbf{\Theta}}} g(\widetilde{\mathbf{\Theta}}_p)$ and the $(p-1)$-th search direction $\mathbf{d}_{p-1}$. Since these two vectors lie in different tangent spaces, they cannot be directly combined. Thus, the Riemannian transport operation is needed to map $\mathbf{d}_{p-1}$ into the tangent space of $\text{grad}_{\widetilde{\mathbf{\Theta}}} g(\widetilde{\mathbf{\Theta}}_p)$. Then, the search direction $\mathbf{d}_p$ is given by

$$\mathbf{d}_p = -\text{grad}_{\widetilde{\mathbf{\Theta}}} g(\widetilde{\mathbf{\Theta}}_p) + \beta_p \mathbf{d}_{p-1}^{\text{t}}, \tag{23}$$

where β_p is the Polak-Ribiere parameter [38] and the superscript "t" indicates the Riemannian transport operation. The step size α_p is chosen by the Armijo backtracking line search method [38] and the p-th update is thus expressed as

$$\widetilde{\mathbf{\Theta}}_p = \text{Retr}_{\widetilde{\mathbf{\Theta}}} \left(\widetilde{\mathbf{\Theta}}_{p-1} + \alpha_p \mathbf{d}_p \right), \tag{24}$$

where $\text{Retr}_{\widetilde{\mathbf{\Theta}}}(\cdot)$ indicates the retraction operation, and it maps the point on the tangent space to the manifold.

After obtaining $\widetilde{\mathbf{\Theta}}^*$, the optimal $\boldsymbol{\theta}^*$ can be constructed as

$$\boldsymbol{\theta}^* = [\widetilde{\mathbf{\Theta}}^*(1,:)]^T + j[\widetilde{\mathbf{\Theta}}^*(2,:)]^T. \tag{25}$$

The RCG algorithm to obtain $\boldsymbol{\theta}^*$ is summarized in Algorithm 1, where $N_{\max}$ is the maximum number of

Algorithm 2 Joint Symbol-Level Precoding and Reflecting Design for the Power Minimization Problem

Input: $\mathbf{h}_k$, $\mathbf{h}_{rk}$, $\mathbf{G}$, Ω, σ_k, Γ_k, B, $N_{\max}$, δ_{th}.
Output: $\boldsymbol{\theta}^*$, $\mathbf{X}^*$.

Initialize $\boldsymbol{\theta}_0$ by (41), $iter = 0$, $\delta = \infty$, $p_{\text{t}} = 0$.
while $iter \leq N_{\max}$ and $\delta \geq \delta_{\text{th}}$ **do**
  $p_{\text{pre}} = p_{\text{t}}$.
  Calculate precoder $\mathbf{x}_m, m = 1, \ldots, \Omega^K$, by (7).
  Obtain infinite resolution RIS phase shifts $\boldsymbol{\theta}$ using Algorithm 1.
  Calculate $\boldsymbol{\theta}_{\text{d}}$ by (26) for the low-resolution RIS phase shifts case.
  $p_{\text{t}} = \|\mathbf{X}\|_F^2$.
  $\delta = \left| \frac{p_{\text{t}} - p_{\text{re}}}{p_{\text{re}}} \right|$.
  $iter = iter + 1$.
end while
$\boldsymbol{\theta}^* = \boldsymbol{\theta}$ or $\boldsymbol{\theta}_{\text{d}}$, $\mathbf{X}^* = \mathbf{X}$.

iterations and δ_{th} is the threshold to judge convergence.

In the realistic RIS implementation, low-resolution digital phase shifters are more hardware-efficient and practical. The discrete phase-shift $\boldsymbol{\theta}_{\text{d}}$ for the RIS using B bits of resolution can thus be calculated by direct quantization, i.e.,

$$\boldsymbol{\theta}_{\text{d}}(n) = \text{round}\left\{ \frac{\boldsymbol{\theta}^*(n)}{2\pi/2^B} \right\} \times \frac{2\pi}{2^B}, \forall n, \tag{26}$$

where $\text{round}\{\cdot\}$ indicates rounding to the nearest integer.

Now, with the previous developments, the joint symbol-level precoding and reflecting design for the power minimization problem is straightforward. Given an initial value $\boldsymbol{\theta}_0$, the symbol-level precoders $\mathbf{x}_m, m = 1, \ldots, \Omega^K$, and the RIS phase shifts $\boldsymbol{\theta}$ are iteratively updated by solving (7) and (8) until convergence is found. This joint symbol-level precoding and reflecting algorithm for the power minimization problem is summarized in Algorithm 2. Selection of an initial $\boldsymbol{\theta}_0$ will be addressed in Section V.

IV. Algorithm for QoS Balancing Problem

In this section, we first formulate the QoS balancing problem for the considered RIS-enhanced MU-MISO system. Then, a similar algorithm is proposed to iteratively solve the symbol-level precoding and reflecting design problems.

As discussed in Section II, the distance between the received noise-free signal and its decision boundaries essentially determines symbol detection performance; larger distances provide stronger robustness against noise, and thus a lower SER. Therefore, we use this distance as the QoS metric and aim at maximizing

the minimum QoS among users with a given power budget. From Fig. 2, we observe that the distance between point D and its decision boundaries (i.e., the positive halves of the x and y axes in this case) can be expressed as

$$\cos\Phi\left[\Re\{\widetilde{r}_{m,k}e^{-j\angle s_{m,k}}\}\tan\Phi-\left|\Im\{\widetilde{r}_{m,k}e^{-j\angle s_{m,k}}\}\right|\right]. \tag{27}$$

Thus, after ignoring the constant term $\cos\Phi$, the QoS balancing problem can be formulated as

$$\max_{\mathbf{X},\boldsymbol{\theta}}\ \min_{m,k}\ \Re\left\{\widetilde{r}_{m,k}e^{-j\angle s_{m,k}}\right\}\tan\Phi-\left|\Im\left\{\widetilde{r}_{m,k}e^{-j\angle s_{m,k}}\right\}\right| \tag{28a}$$

$$\text{s.t.}\quad \widetilde{r}_{m,k}=\left(\mathbf{h}_k^H+\mathbf{h}_{\mathrm{r}k}^H\boldsymbol{\Theta}\mathbf{G}\right)\mathbf{x}_m,\forall k,\forall m, \tag{28b}$$

$$\boldsymbol{\Theta}=\mathrm{diag}\{\boldsymbol{\theta}\},|\theta_n|=1,\forall n, \tag{28c}$$

$$\|\mathbf{X}\|^2\le P\Omega^K, \tag{28d}$$

where P is the preset average transmit power budget. Similarly, we propose to decompose this bivariate problem into separate symbol-level precoding design and the reflecting design problems, and solve them iteratively.

A. Symbol-Level Precoding Design for QoS Balancing Problem

With given RIS phase shifts $\boldsymbol{\theta}$, the combined channel vector from BS to the k-th user is $\widetilde{\mathbf{h}}_k^H\triangleq\mathbf{h}_k^H+\mathbf{h}_{\mathrm{r}k}^H\boldsymbol{\Theta}\mathbf{G}$. Then, the QoS balancing problem for designing the precoder $\mathbf{X}$ can be rewritten as

$$\max_{\mathbf{X},t}\quad t \tag{29a}$$

$$\text{s.t.}\quad \Re\{\widetilde{\mathbf{h}}_k^H\mathbf{x}_m e^{-j\angle s_{m,k}}\}\tan\Phi-\left|\Im\{\widetilde{\mathbf{h}}_k^H\mathbf{x}_m e^{-j\angle s_{m,k}}\}\right|\ge t,\forall k,\forall m, \tag{29b}$$

$$\|\mathbf{X}\|^2\le P\Omega^K, \tag{29c}$$

which is a convex problem and can be solved by standard convex optimization tools, e.g. CVX. However, since the variable to be optimized $\mathbf{X}$ has a large dimension of $N\Omega^K$, the complexity is unaffordable. In order to deal with this difficulty, we decompose this problem into Ω^K sub-problems, where $\mathbf{x}_m,\forall m$, is individually designed. To facilitate the algorithm development, we propose the following proposition.

Proposition 1. *Let* $\mathbf{x}_1^*,\ldots,\mathbf{x}_{\Omega^K}^*$ *be the optimal solution of the QoS balancing problem (29). Let* $\mathbf{x}_1^\star,\ldots,\mathbf{x}_{\Omega^K}^\star$

be the optimal solution of the power minimization problem (7), where the QoS requirement for all users equals $t_0 = \sigma_k\sqrt{\Gamma_k}\tan\Phi, \forall k$. *Then,* $\mathbf{x}_m^*$ *is a scaled version of* $\mathbf{x}_m^\star$, *i.e.,* $\mathbf{x}_m^* = \frac{\sqrt{P_m}\mathbf{x}_m^\star}{\|\mathbf{x}_m^\star\|}$, *where* $P_m \geq 0$ *is the transmit power allocated to the* m*-th precoder,* $\sum_{m=1}^{\Omega^K} P_m = P\Omega^K$. *Furthermore, the minimum QoS that* $\mathbf{x}_m^*$ *can achieve is* $\frac{\sqrt{P_m}t_0}{\|\mathbf{x}_m^\star\|}$.

Proof. See Appendix A. □

Proposition 1 indicates that we can first find the precoder $\mathbf{x}_m^\star$ by individually solving the power minimization problem (7) with a given QoS requirement t_0, and then scaling $\mathbf{x}_m^\star$ appropriately to obtain the optimal $\mathbf{x}_m^*$ by finding the optimal power allocation P_m. With given $\mathbf{x}_m^\star$, the power allocation problem to optimize QoS balancing can be formulated as

$$\max_{P_m,\forall m} \quad t \tag{30a}$$

$$\text{s.t.} \quad t \leq \frac{\sqrt{P_m}t_0}{\|\mathbf{x}_m^\star\|}, \forall m, \tag{30b}$$

$$\sum_{m=1}^{\Omega^K} P_m \leq P\Omega^K. \tag{30c}$$

While (30) is convex and can be solved by CVX, we attempt to find a more efficient solution to reduce the complexity. Denoting $\mathbf{p} \triangleq \left[\sqrt{P_1}, \ldots, \sqrt{P_{\Omega^K}}\right]^T$, the power allocation problem (30) can be rewritten as

$$\max_{\mathbf{p},t} \quad t \tag{31a}$$

$$\text{s.t.} \quad t \leq \mathbf{e}_m^T\mathbf{p}, \forall m, \tag{31b}$$

$$\|\mathbf{p}\|^2 \leq P\Omega^K, \tag{31c}$$

where $\mathbf{e}_m$ is a vector of all zeros except the m-th element which is $\frac{t_0}{\|\mathbf{x}_m^\star\|}$. Motivated by Proposition 1, we first find $\mathbf{p}^\star$, which is the optimal solution for the following power minimization problem with an arbitrary given $t_0' \geq 0$:

$$\min_{\mathbf{p}} \quad \|\mathbf{p}\|^2 \tag{32a}$$

$$\text{s.t.} \quad \mathbf{e}_m^T\mathbf{p} \geq t_0', \forall m. \tag{32b}$$

This problem can be efficiently solved using the same method for problem (7), based on the Lagrangian dual problem and exploiting the gradient projection algorithm. Then, the optimal $\mathbf{p}^*$ for (32) can be obtained by $\mathbf{p}^* = \frac{\sqrt{P\Omega^K}\mathbf{p}^\star}{\|\mathbf{p}^\star\|}$.

With the above analysis, the symbol-level precoing algorithm for the QoS balancing problem can be summarized as: *i*) obtain the precoder $\mathbf{x}_m^\star$ by solving the power minimization problem (7) with a certain QoS requirement $t_0 \geq 0$; *ii*) solving the power allocation problem (30) to obtain $P_m, \forall m$; *iii*) scaling $\mathbf{x}_m^\star$ to obtain the optimal solution of (29) as $\mathbf{x}_m^* = \frac{\sqrt{P_m}\mathbf{x}_m^\star}{\|\mathbf{x}_m^\star\|}$.

B. Reflecting Design for QoS Balancing Problem

With fixed precoders $\mathbf{x}_1, \ldots, \mathbf{x}_{\Omega^K}$, the reflecting design problem is given by

$$\max_{\boldsymbol{\theta}} \min_{m,k} \Re\{\widetilde{r}_{m,k} e^{-j\angle s_{m,k}}\} \tan\Phi - \left|\Im\{\widetilde{r}_{m,k} e^{-j\angle s_{m,k}}\}\right| \tag{33a}$$

$$\text{s.t.} \quad \widetilde{r}_{m,k} = \left(\mathbf{h}_k^H + \mathbf{h}_{\mathrm{r}k}^H \boldsymbol{\Theta}\mathbf{G}\right)\mathbf{x}_m, \forall k, \forall m, \tag{33b}$$

$$\boldsymbol{\Theta} = \mathrm{diag}\{\boldsymbol{\theta}\}, |\theta_n| = 1, \forall n. \tag{33c}$$

Using the definitions in (9), the reflecting design problem is more compactly formulated as

$$\min_{\boldsymbol{\theta}} \quad \max_{m,k} \quad |\Im\{\widehat{r}_{m,k}\}| - \Re\{\widehat{r}_{m,k}\} \tan\Phi \tag{34a}$$

$$\text{s.t.} \quad |\theta_n| = 1, \forall n. \tag{34b}$$

As before, (34a) is non-differentiable due to the max and absolute value functions and (34b) is non-convex, which leads us to exploit the RCG algorithm. To facilitate the RCG algorithm, the same idea used to solve (10a) is employed here in three steps: *i*) replacing the absolute value function, *ii*) smoothing the max function, *iii*) calculating its Euclidean gradient. We briefly describe these three steps below.

The absolute value function is replaced using (11), and the problem is further rearranged as

$$\min_{\widetilde{\boldsymbol{\Theta}}} \quad \max_{i} \quad f_i \tag{35a}$$

$$\text{s.t.} \quad [\widetilde{\boldsymbol{\Theta}}(:,n)]^T \widetilde{\boldsymbol{\Theta}}(:,n) = 1, \forall n, \tag{35b}$$

where f_i is defined in (14) with the auxiliary vectors $\mathbf{a}_{2i-1}$, $\mathbf{b}_{2i-1}$, $\mathbf{a}_{2i}$ $\mathbf{b}_{2i}$ in (15a), (15b), (15d), (15e), and

$$c_{2i-1} \triangleq \Im\{a_{m,k}\} - \Re\{a_{m,k}\} \tan \Phi, \tag{36a}$$

$$c_{2i} \triangleq -\Im\{a_{m,k}\} - \Re\{a_{m,k}\} \tan \Phi. \tag{36b}$$

We smooth the max function by exploiting the log-sum-exp algorithm, which introduces the approximation

$$\max\{f_1, f_2, \ldots, f_{2\Omega^K}\} \approx g(\widetilde{\boldsymbol{\Theta}}) \triangleq \varepsilon \log \left\{ \sum_{i=1}^{K\Omega^K} \left[\exp\left(\frac{f_{2i-1}}{\varepsilon}\right) + \exp\left(\frac{f_{2i}}{\varepsilon}\right) \right] \right\}, \tag{37}$$

where ε is a small positive number.

After obtaining the smooth and differentiable $g(\widetilde{\boldsymbol{\Theta}})$, its Euclidean gradient can be derived by substituting (20) into (19), where we need to calculate

$$\frac{\partial g}{\partial \Re\{\boldsymbol{\theta}^H\}} = \frac{\sum_{i=1}^{K\Omega^K} \left[\exp(f_{2i-1}/\varepsilon)\mathbf{a}_{2i-1}^T + \exp(f_{2i}/\varepsilon)\mathbf{a}_{2i}^T\right]}{\sum_{i=1}^{K\Omega^K} \left[\exp(f_{2i-1}/\varepsilon) + \exp(f_{2i+1}/\varepsilon)\right]}, \tag{38a}$$

$$\frac{\partial g}{\partial \Im\{\boldsymbol{\theta}^H\}} = \frac{\sum_{i=1}^{K\Omega^K} \left[\exp(f_{2i-1}/\varepsilon)\mathbf{b}_{2i-1}^T + \exp(f_{2i}/\varepsilon)\mathbf{b}_{2i}^T\right]}{\sum_{i=1}^{K\Omega^K} \left[\exp(f_{2i-1}/\varepsilon) + \exp(f_{2i+1}/\varepsilon)\right]}. \tag{38b}$$

Then, the RCG-based reflecting design in Algorithm 1 can be applied to solve the QoS balancing problem. The optimal RIS phase shifts $\boldsymbol{\theta}^*$ and low-resolution phase shifts $\boldsymbol{\theta}_{\mathrm{d}}$ have the same format as in (25) and (26).

Finally, the joint symbol-level precoding and reflecting design for the QoS balancing problem is straightforward. With an initial reflecting value $\boldsymbol{\theta}_0$, the symbol-level precoding matrix $\mathbf{X}$ and the RIS phase shifts $\boldsymbol{\theta}$ are iteratively updated by solving (29) and (33) until convergence is found.

V. Initialization and Complexity Analysis

A. Initialization

Since the RCG algorithm in general will find a locally optimal solution, an initial value that is close to the optimal solution can provide better performance and accelerate convergence. In this subsection, we propose a heuristic method to obtain the initial $\boldsymbol{\theta}_0$.

Both the power minimization and QoS balancing problems depend on the quality of the users' channels, which can be manipulated by RIS. Therefore, without considering the precoding, we can simply design the RIS phase shifts to maximize the minimum channel gain for all users:

$$\max_{\boldsymbol{\theta}_0} \ \min_{k} \quad \left\|\mathbf{h}_k^H + \mathbf{h}_{\mathrm{r}k}^H \boldsymbol{\Theta}_0 \mathbf{G}\right\|^2 \tag{39a}$$

$$\text{s.t.} \quad \boldsymbol{\Theta}_0 = \mathrm{diag}\{\boldsymbol{\theta}_0\}, |\theta_n| = 1, \forall n. \tag{39b}$$

By introducing two auxiliary variables β and μ, (39) can be rearranged as

$$\max_{\overline{\boldsymbol{\theta}}_0} \quad \beta \tag{40a}$$

$$\text{s.t.} \quad \beta \leq \overline{\boldsymbol{\theta}}_0^H \mathbf{R}_k \overline{\boldsymbol{\theta}}_0 + \left\|\mathbf{h}_k\right\|^2, \forall k, \tag{40b}$$

$$\left|\overline{\boldsymbol{\theta}}_0(n)\right| = 1, n = 1, \ldots, N+1, \tag{40c}$$

where $\overline{\boldsymbol{\theta}}_0 \triangleq [\boldsymbol{\theta}_0; \mu]$, $\mathbf{G}_k \triangleq \mathrm{diag}\{\mathbf{h}_{\mathrm{r}k}\}\mathbf{G}$, and $\mathbf{R}_k \triangleq \begin{bmatrix} \mathbf{G}_k \mathbf{G}_k^H & \mathbf{G}_k \mathbf{h}_k \\ \mathbf{h}_k^H \mathbf{G}_k^H & 0 \end{bmatrix}$. It is noted that (40) is a quadratically constrained quadratic program (QCQP) problem, which can be solved by the semidefinite relaxation (SDR) algorithm [39]. In particular, defining $\overline{\boldsymbol{\Theta}}_0 \triangleq \overline{\boldsymbol{\theta}}_0 \overline{\boldsymbol{\theta}}_0^H$, (40) is converted to

$$\max_{\overline{\boldsymbol{\Theta}}_0} \quad \beta \tag{41a}$$

$$\text{s.t.} \quad \beta \leq \mathrm{trace}\left\{\mathbf{R}_k \overline{\boldsymbol{\Theta}}_0\right\} + \left\|\mathbf{h}_k\right\|^2, \forall k, \tag{41b}$$

$$\overline{\boldsymbol{\Theta}}_0(n,n) = 1, n = 1, \ldots, N+1, \tag{41c}$$

$$\overline{\boldsymbol{\Theta}}_0 \succeq \mathbf{0}, \mathrm{rank}\{\overline{\boldsymbol{\Theta}}_0\} = 1. \tag{41d}$$

Ignoring the rank-one constraint, (41) is a semidefinite program (SDP) problem and can be solved using standard convex optimization tools such as the CVX solver [36]. If the obtained solution satisfies the rank-one constraint, $\boldsymbol{\theta}_0$ can be calculated via an eigenvalue decomposition. Otherwise, the Gaussian randomization algorithm is applied to provide an approximate solution.

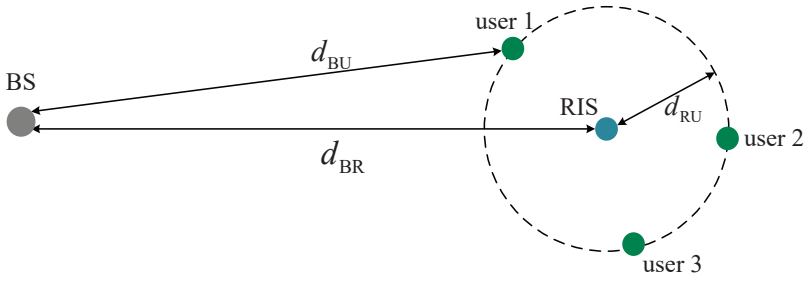

Fig. 3: Simulation setup for multiuser case.

B. Complexity

In this subsection, we provide a brief complexity analysis for the proposed joint symbol-level precoding and reflecting design algorithms. The complexity to obtain the initial $\boldsymbol{\theta}_0$ is at most $\mathcal{O}\{\sqrt{K(N+1)}[K^3(N+1)^2+K^2(N+1)^3]\}$ using the CVX solver. For the power minimization problem, the complexity to solve for precoder $\mathbf{x}_m$ by the gradient projection algorithm is $\mathcal{O}\{M^3\}$, and the worst-case computation for the RCG algorithm is of order $\mathcal{O}\{(2N)^{1.5}\}$. Therefore, the total computational complexity of Algorithm 2 is $\mathcal{O}\{\sqrt{K(N+1)}[K^3(N+1)^2+K^2(N+1)^3]+N_{\max}[\Omega^K M^3+(2N)^{1.5}]\}$. The symbol-level precoding algorithm for the QoS balancing problem is derived by solving the corresponding power minimization problem, and the reflecting designs for these two problems are similar. Thus, the complexity to solve the QoS balancing problem is the same as the power minimization problem.

VI. Simulation Results

In this section, we provide extensive simulation results to illustrate the effectiveness of our proposed algorithms. For simplicity, we assume QPSK modulation ($\Omega = 4$) is used. The QoS requirement and the noise power for $K = 3$ users is the same, i.e., $\Gamma = \Gamma_k, \forall k, \sigma^2 = \sigma_k^2 = -80$dBm, $\forall k$. The transmit antenna array at the BS is assumed to be a uniform linear array with antenna spacing given by $\lambda/2$. The distance-dependent path loss modeled as $\mathrm{PL}(d) = C_0\left(\frac{d}{d_0}\right)^{-\alpha}$, where $C_0 = -30$dB is the path loss for the reference distance $d_0 = 1$m, d is the link distance, and α is the path-loss factor. In addition, the small-scale Rician fading channel model for all channels is assumed, which consists of line of sight (LoS) and not line of sight (NLoS) components. The channels from the BS to the RIS can be expressed as

$$\mathbf{G} = \sqrt{\frac{\kappa}{\kappa+1}}\mathbf{G}^{\mathrm{LoS}} + \sqrt{\frac{1}{\kappa+1}}\mathbf{G}^{\mathrm{NLoS}}, \tag{42}$$

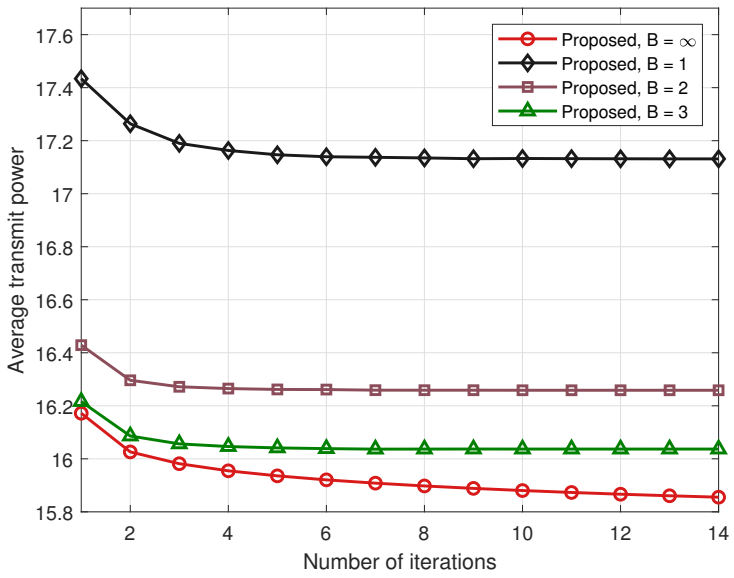

Fig. 4: Average transmit power versus the number of iterations ($K = 3$ users, $N = 64$ reflecting elements, $M = 6$ transmit antennas, $\Gamma = 10$ dB).

where κ is the Rician factor set as 3dB, $\mathbf{G}^{\mathrm{LoS}}$ is the LoS component depends on the geometric settings, and $\mathbf{G}^{\mathrm{NLoS}}$ is the NLoS Rayleigh fading component. The MISO channels $\mathbf{h}_k$ and $\mathbf{h}_{\mathrm{r}k}, k = 1, \ldots, K$, have the similar model, which consist of LoS and NLoS components.

The geometric location for the following simulations is shown in Fig. 3, where the top of view is plotted. In general, RIS is deployed far away from the BS to provide significant performance improvement for its nearby users, who may suffer from blockage and serve attenuation. Therefore, we set the distance between the BS and the RIS $d_{\mathrm{BR}} = 50$m, the distance between the RIS and the users $d_{\mathrm{RU}} = 3$m, and the distance between the BS and each user d_{BU} lies in the interval $[d_{\mathrm{BR}} - d_{\mathrm{RU}}, d_{\mathrm{BR}} + d_{\mathrm{RU}}]$. The users are randomly distributed on the dashed circle line in Fig. 3. Considering the link distance, the path-loss factors for $\mathbf{h}_k$, $\mathbf{h}_{\mathrm{r}k}$ and $\mathbf{G}$ are set as 3.5, 2.8, and 2.5, respectively, to simulate a more practical scenario.

A. Power Minimization Problem

In this subsection, we illustrate the simulation results for the power minimization problem. We first show in Fig. 4 the convergence of our proposed algorithm for the cases where the RIS has continuous, 1-bit, 2-bit, and 3-bit phase shifters, i.e., $B = \infty, 1, 2, 3$, respectively. It can be observed that our proposed algorithm converges very quickly, particularly for the low-resolution cases. These convergence results are encouraging for a low complexity implementation.

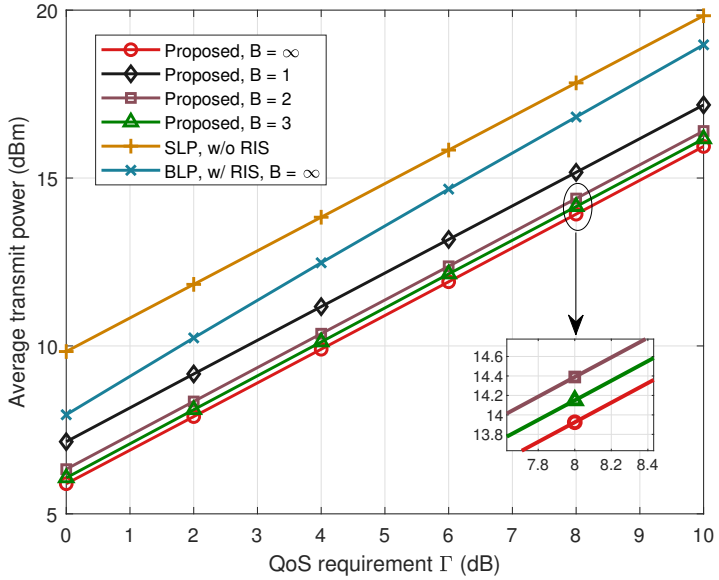

Fig. 5: Average transmit power versus QoS requirement Γ ($K = 3$ users, $N = 64$ reflecting elements, $M = 6$ transmit antennas).

In Fig. 5, we show the average transmit power versus the QoS requirement Γ. In order to demonstrate the effectiveness of our proposed joint symbol-level precoding and reflecting design, we also include: *i*) Symbol-level precoding without the aid of the RIS (denoted as "SLP, w/o RIS"); *ii*) block-level precoding with the aid of RIS and continuous phase shifters [10] (denoted as "BLP, w/ RIS, $B = \infty$"). It can be seen from Fig. 5 that our proposed scheme requires less transmit power than the "SLP, w/o RIS" approach, which validates the effectiveness of RIS in the symbol-level precoding systems. We can also observe that the proposed joint symbol-level precoding and reflecting algorithm outperforms the "BLP, w/ RIS, $B = \infty$" approach, which verifies the performance improvement due to symbol-level precoding. In addition, it is noted that with the increasing B, better system performance can be achieved. Moreover, the 3-bit scheme can provide satisfactory performance as the ideal unquantized solution, which indicates that the 3-bit scheme can provide a favorable trade-off between cost and performance. Beyond $B = 3$ bits, the extra cost and complexity associated with using higher-resolution RIS are not warranted given the very marginal increase in system performance.

Next, we present the average transmit power versus the number of reflecting elements N in Fig. 6. The same relationship can be observed as in Fig. 5. We observe that as the number of reflecting elements increases, the average transmit power is greatly reduced, and the reduction is more pronounced for our

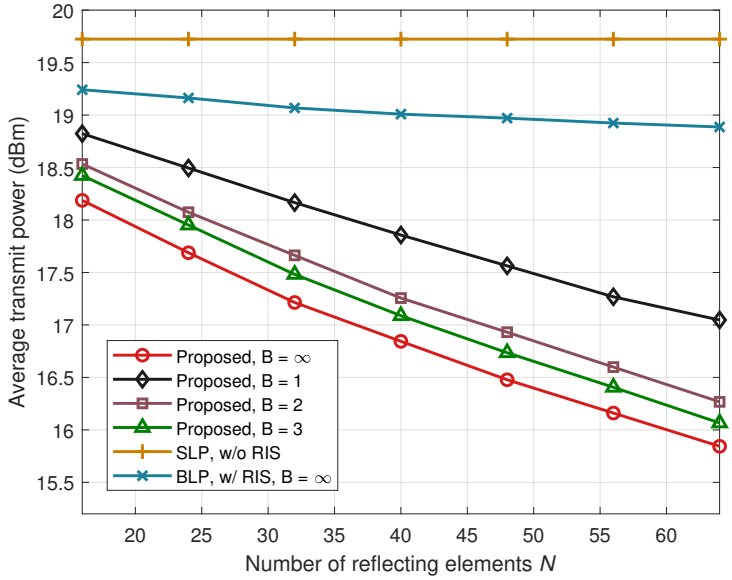

Fig. 6: Average transmit power versus the number of reflecting elements N ($K = 3$ users, $M = 6$ transmit antennas, $\Gamma = 10$ dB).

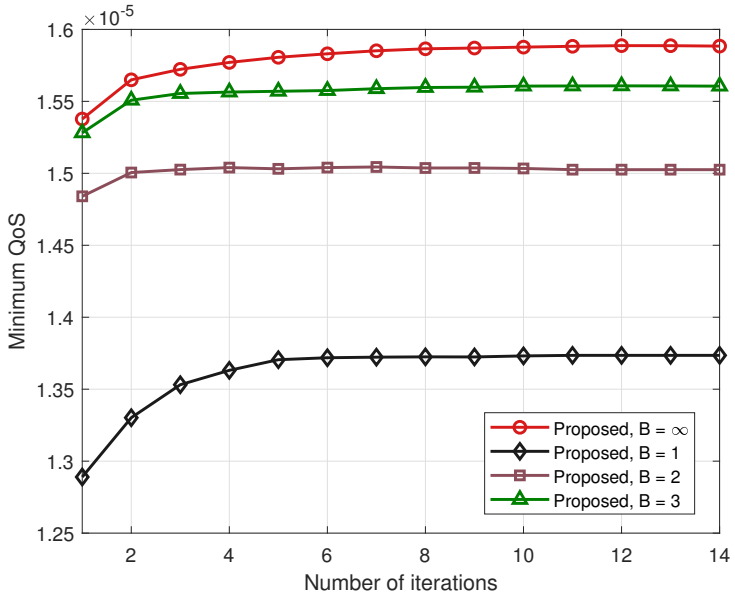

Fig. 7: Minimum QoS versus the number of iterations ($K = 3$ users, $N = 64$ reflecting elements, $M = 6$ transmit antennas, $P = 20$ dBm).

proposed SLP algorithms compared with block-level precoding. This supports the main idea of our paper, that the combination of SLP and RIS provides symbiotic benefits.

B. QoS Balancing Problem

In this subsection, we present simulations for the QoS balancing problem. The convergence performance is similar to that observed for the power minimization problem in Fig. 7. It is seen that all schemes have

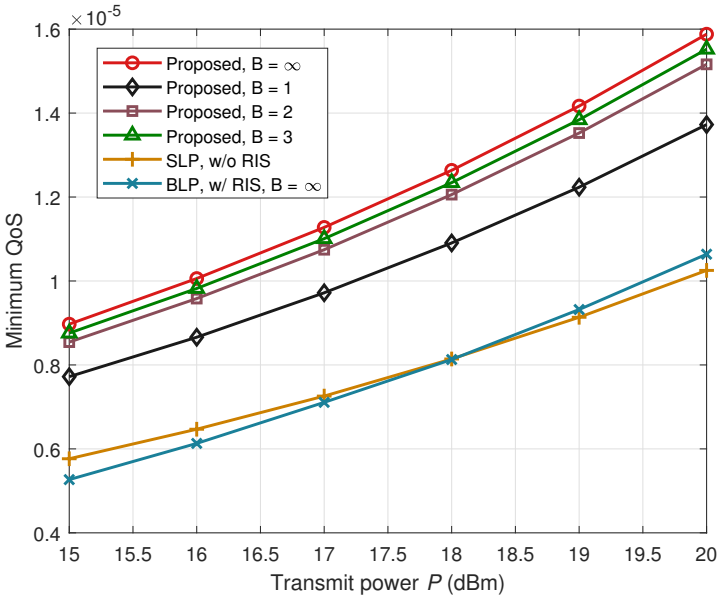

Fig. 8: Minimum QoS versus the transmit power P ($K = 3$ users, $N = 64$ reflecting elements, $M = 6$ transmit antennas).

very fast convergence, which provides favorable computational complexity.

In Fig. 8, we plot the worst-case performance t achieved for the QoS balancing problem versus the transmit power P. As the transmit power increases, the minimum QoS of all methods increases, which means that the distance between the received noise-free signal and its decision boundaries becomes larger. The minimum QoS achieved by our proposed joint symbol-level precoding and reflecting algorithm is dramatically larger than the other two competitors, which further supports the benefit of using RIS together with symbol-level precoding.

In order to demonstrate the QoS improvement in a more intuitive and natural way with a familiar metric, in Fig. 9 we present the average SER versus the transmit power. Obviously, the larger QoS requirement (i.e., Γ), which results in the larger distance between the received signal and its decision boundaries, leads to better performance in terms of a lower SER. This relationship can be verified by comparing Figs. 9 and 8. More importantly, the improvement in the SER performance of our proposed algorithm is also very remarkable. When the 3-bit RIS can offer close to 10^{-4} SER, the symbol-level precoding system without RIS provides only 10^{-2} SER. Therefore, utilizing the QoS requirement Γ as the performance metric for optimizing the RIS-enhanced symbol-level precoding systems is reasonable and effective.

Next, we show the average SER versus the number of reflecting elements N in Fig. 10. Since the

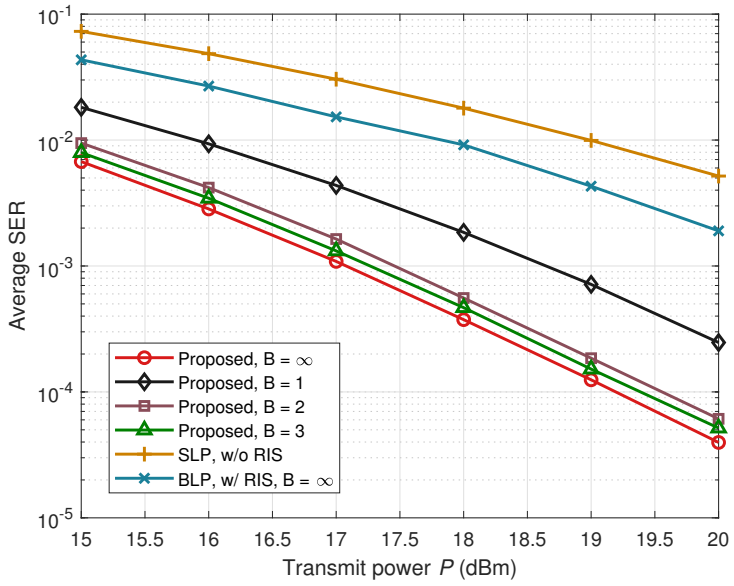

Fig. 9: Average SER versus the transmit power P ($K = 3$ users, $N = 64$ reflecting elements, $M = 6$ transmit antennas).

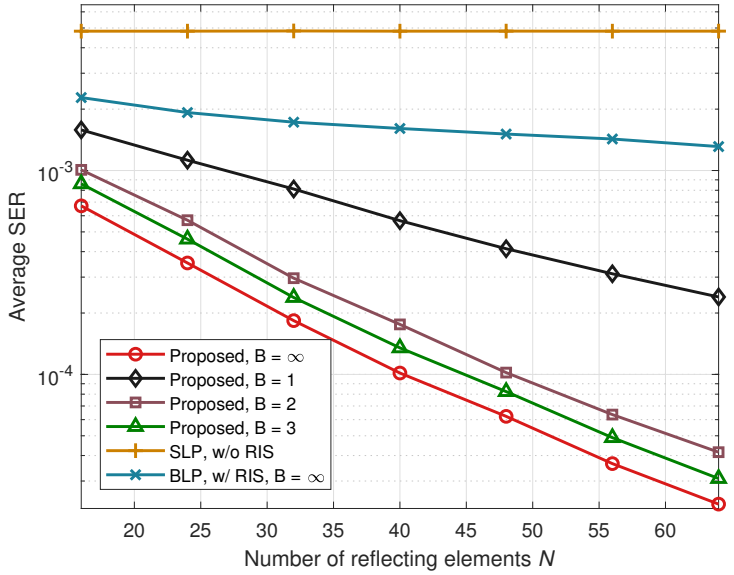

Fig. 10: Average SER versus the number of reflecting elements N ($K = 3$ users, $N = 64$ reflecting elements, $M = 6$ transmit antennas, $P = 20$ dBm).

larger RIS can provide larger beamforming/reflecting gains, we observe that the average SER decreases for all schemes with increasing N. Moreover, our proposed schemes always achieve significantly better SER performance for different RIS sizes.

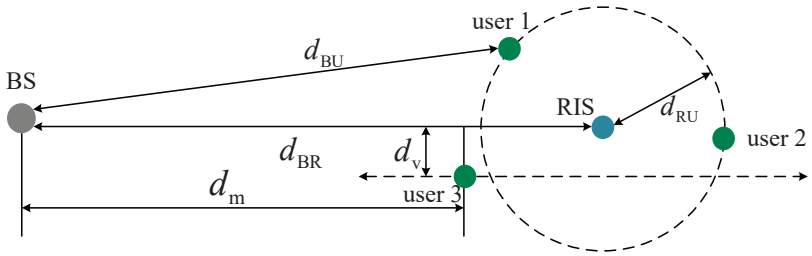

Fig. 11: Simulation setup for mobile user case.

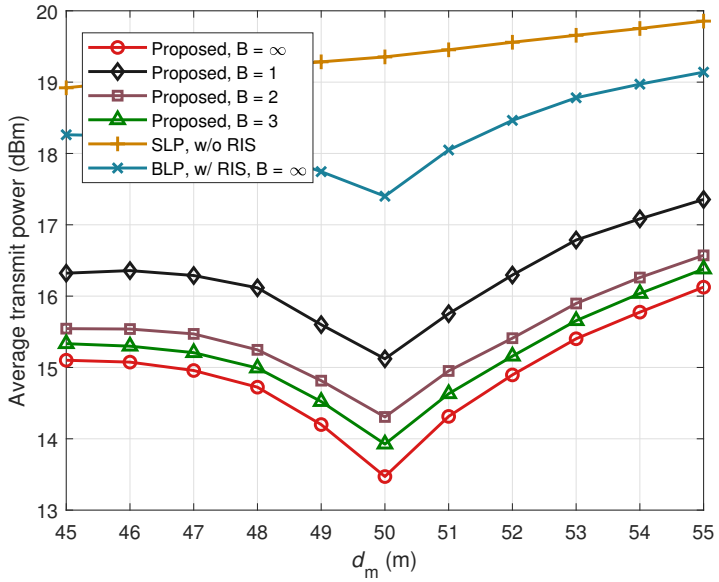

Fig. 12: Average transmit power versus d_{m} ($K = 3$ users, $N = 64$ reflecting elements, $M = 6$ transmit antennas, SNR $= 10$ dB).

C. Impact of RIS Location

Finally, in order to demonstrate the impact of RIS location, we simulate a case where the position of one of the users changes along a horizontal line parallel to the line between the BS and RIS. As shown in Fig. 11, user 3 moves along the dashed line and the vertical distance between it and the BS-RIS link is $d_{\mathrm{v}} = 0.5$m. Let d_{m} be the horizontal distance between the BS and user 3. The other two users are still located 3m from the RIS. In Figs. 11 and 12, we show the system performance as a function of d_{m}. We observe that the RIS-enhanced system has the best performance when the user moves closest to the RIS and the other two users, i.e., $d_{\mathrm{m}} = 50$m, since a larger reflection gain is obtained when the user is closest to the RIS. Moreover, when the users move closer together, MUI may become stronger, which can be effectively exploited by symbol-level precoding.

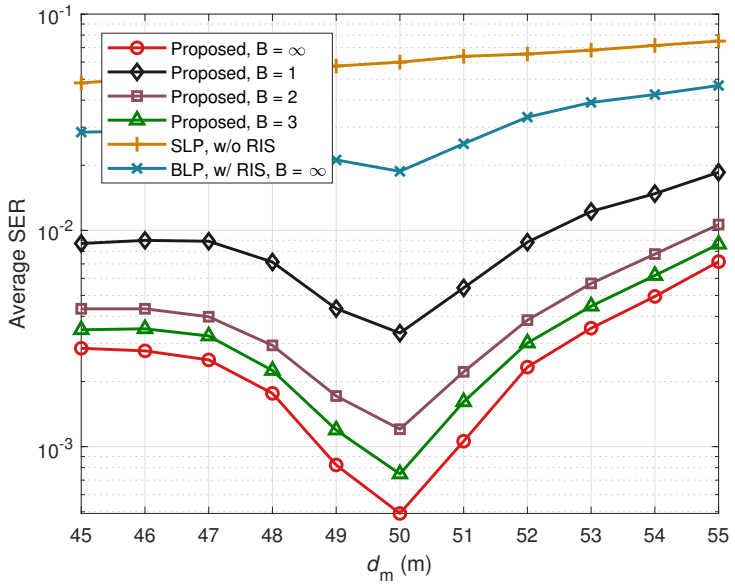

Fig. 13: Average SER versus d_{m} ($K = 3$ users, $N = 64$ reflecting elements, $M = 6$ transmit antennas, $P = 15$ dBm).

VII. Conclusions

In this paper, we investigated RIS-enhanced wireless networks, where an IRS is deployed to assist the multi-user MISO communication system, which employs symbol-level precoding to exploit the multi-user interference. In particular, we considered the joint symbol-level precoding and reflecting design problems for RIS-enhanced MU-MISO systems. Efficient iterative algorithms were proposed to solve the power minimization and QoS balancing problems. The gradient-projection-based and Riemannian conjugate gradient (RCG)-based algorithms were used to design symbol-level precoding and RIS phase shifts, respectively. The simulation results illustrated that our proposed algorithms exhibit remarkably better performance in terms of power-savings and SER-reductions. These positive results have confirmed that the employment of RIS in symbol-level precoding systems can provide more efficient multi-user interference exploitation by intelligently manipulating the multi-user channels.

Appendix A

Proof of Proposition 1. We assume the optimal solution of the QoS balancing problem (29) is $\mathbf{x}_m^*, \forall m$, and t^*, and we denote the transmit power allocated to the m-th precoder as $P_m \triangleq \|\mathbf{x}_m^*\|^2$. If the power

allocations $P_m, \forall m$, are known, the QoS balancing problem can be divided into Ω^K sub-problems and the m-th sub-problem is written as

$$\max_{\mathbf{x}_m, t_m} \quad t_m \tag{43a}$$

$$\text{s.t.} \quad \Re\{\widetilde{\mathbf{h}}_k^H \mathbf{x}_m e^{-j\angle s_{m,k}}\} \tan\Phi - \left|\Im\{\widetilde{\mathbf{h}}_k^H \mathbf{x}_m e^{-j\angle s_{m,k}}\}\right| \geq t_m, \forall k, \tag{43b}$$

$$\|\mathbf{x}_m\|^2 \leq P_m. \tag{43c}$$

It can be easily verified that the inequality constraint (43c) holds with equality at the optimal $\mathbf{x}_m^*$. Moreover, $\mathbf{x}_m^*$ is also the the optimal solution for the following power minimization problem:

$$\min_{\mathbf{x}_m} \quad \|\mathbf{x}_m\|^2 \tag{44a}$$

$$\text{s.t.} \quad \Re\{\widetilde{\mathbf{h}}_k^H \mathbf{x}_m e^{-j\angle s_{m,k}}\} \tan\Phi - \left|\Im\{\widetilde{\mathbf{h}}_k^H \mathbf{x}_m e^{-j\angle s_{m,k}}\}\right| \geq t_m^*, \forall k. \tag{44b}$$

To prove this statement by contradiction, we start by assuming that $\mathbf{x}_m^*$ is not optimal for (44) and there exists another $\overline{\mathbf{x}}_m$ satisfying (44b) and requiring less power, i.e. $\|\overline{\mathbf{x}}_m\| < P_m$. Then, we can scale up $\overline{\mathbf{x}}_m$ to let the power constraint (43c) become equal and provide a higher t_m in (43), in which case $\mathbf{x}_m^*$ is not optimal any more, and this results in contradiction.

If we use an arbitrary $t_0 > 0$ as the QoS requirement in (44b) instead of t_m^*, the optimal solution $\mathbf{x}_m^\star$ of this power minimization problem is the scaled version of $\mathbf{x}_m^*$, since the constraint (44b) is a linear function. More specifically, $\mathbf{x}_m^* = \frac{\sqrt{P_m}\mathbf{x}_m^\star}{\|\mathbf{x}_m^\star\|}$ with the optimal power P_m.

If we set the QoS requirement as $t_0 = \sigma_k\sqrt{\Gamma_k}\tan\Phi$, then (44) has the same format as (7), which implies that the optimal $\mathbf{x}_m^\star$ for the power minimization problem (7) is also a scaled version of the optimal $\mathbf{x}_m^*$ for the QoS balancing problem (29). Proposition 1 is therefore proved.

□

REFERENCES

[1] S. Zhang, Q. Wu, S. Xu, and G. Y. Li, "Fundamental green tradeoffs: Progress, challenges, and impacts on 5G networks," *IEEE Commun. Surveys Tuts.*, vol. 19, no. 1, pp. 33-56, First Quarter 2017.

[2] A. L. Swindlehurst, E. Ayanoglu, P. Heydari, and F. Capolino, "Millimeter-wave massive MIMO: The next wireless revolution?" *IEEE Commun. Mag.*, vol. 52, no. 9, pp. 56-62, Sept. 2014.

[3] C. Liaskos, S. Nie, A. Tsioliaridou, A. Pitsillides, S. Ioannidis, and I. Akyildiz, "A new wireless communication paradigm through software-controlled metasurfaces," *IEEE Commun. Mag.,* vol. 56, no. 9, pp. 162-169, Sept. 2018.

[4] E. Basar, M. D. Renzo, J. d. Rosny, M. Debbah, M.-S. Alouini, and R. Zhang, "Wireless communications through reconfigurable intelligent surfaces," *IEEE Access*, vol. 7, pp.116753-116773, Aug. 2019.

[5] M. D. Renzo, *et al.*, "Smart radio environments empowered by AI reconfigurable meta-surfaces: An idea whose time has come," March 2019. [Online]. Avaliable: https://arXiv.org/abs/1903.08925

[6] J. Zhao and Y. Li, "A survey of intelligent reflecting surfaces (IRSs): Towards 6G wireless communication networks," Nov. 2019. [Online]. Avaliable: https://arXiv.org/abs/1907.04789

[7] J. Zhao, "Optimizations with intelligent reflecting surfaces (IRSs) in 6G wireless networks: Power control, quality of service, max-min fair beamforming for unicast, broadcast, and multicast with multi-antenna mobile users and multiple IRSs," Aug. 2019. [Online]. Avaliable: https://arXiv.org/abs/1908.03965

[8] Q. Wu and R. Zhang, "Beamforming optimization for intelligent reflecting surface with discrete phase shifts," in *Proc. IEEE Int. Conf. Acoust. Speech Signal Process. (ICASSP)*, Brighton, United Kingdom, May 2019.

[9] Q. Wu and R. Zhang, "Intelligent reflecting surface enhanced wireless network: Joint active and passive beamforming design," in *Proc. IEEE Global Commun. Conf. (GLOBECOM)*, Abu Dhabi, United Arab Emirates, Dec. 2018.

[10] Q. Wu and R. Zhang, "Intelligent reflecting surface enhanced wireless network via joint active and passive beamforming," *IEEE Trans. Wireless Commun.*, vol. 18, no. 11, pp. 5394-5409, Nov. 2019.

[11] H. Han, J. Zhao, D. Niyato, M. D. Renzo, and Q.-V. Pham, "Intelligent reflecting surface aided network: Power control for physical-layer broadcasting," Nov. 2019. [Online]. Avaliable: https://arXiv.org/abs/1910.14383

[12] X. Yu, D. Xu, and R. Schober, "MISO wireless communication systems via intelligent reflecting surfaces," in *Proc. IEEE/CIC Int. Conf. Commun. in China (ICCC)*, Changchun, China, Aug. 2019.

[13] Q.-U.-A. Nadeem, A. Kammoun, A. Chaaban, M. Debbah, and M.-S. Alouini, "Asymptotic analysis of large intelligent surface assisted MIMO communication," April 2019. [Online]. Avaliable: https://arXiv.org/abs/1903.08127

[14] Q. Wu and R. Zhang, "Weighted sum power maximization for intelligent reflecting surface aided SWIPT," Sept. 2019. [Online]. Avaliable: https://arXiv.org/abs/1907.05558

[15] Y. Han, W. Tang, S. Jin, C.-K. Wen, and X. Ma, "Large intelligent surface-assisted wireless communication statistical CSI," *IEEE Trans. Veh. Technol.*, vol. 68, no. 8, pp. 8238-8242, Aug. 2018.

[16] J. Ye, S. Guo, and M.-S. Alouini, "Joint reflecting and precoding designs for SER minimization in reconfigurable intelligent surfaces assisted MIMO systems," June 2019. [Online]. Avaliable: https://arXiv.org/abs/1906.11466

[17] N. S. Perović, M. D. Renzo, and M. F. Flanagan, "Channel capacity optimization using reconfigurable intelligent surfaces in indoor mmWave environments," Oct. 2019. [Online]. Avaliable: https://arXiv.org/abs/1910.14310

[18] S. Li, B. Duo, X. Yuan, Y.-C. Liang, and M. D. Renzo, "Reconfigurable intelligent surface assisted UAV communication: Joint trajectory design and passive beamforming," Aug. 2019. [Online]. Avaliable: https://arXiv.org/abs/1908.04802

[19] M. Jung, W. Saad, M. Debbah, and C. S. Hong, "On the optimality of reconfigurable intelligent surfaces (RISs): Passive beamforming, modulation, and resource allocation," Oct. 2019. [Online]. Avaliable: https://arXiv.org/abs/1910.00968

[20] C. Pan, H. Ren, K. Wang, W. Xu, M. Elkashlan, A. Nallanathan, and L. Hanzo, "Multicell MIMO communications relying on intelligent

reflecting surface," Aug. 2019. [Online]. Avaliable: https://arXiv.org/abs/1907.10864

[21] C. Huang, A. Zappone, G. C. Alexandropoulos, M. Debbah, and C. Yuen, "Reconfigurable intelligent surfaces for energy efficiency in wireless communication," *IEEE Trans. Wireless Commun.*, vol. 18, no.8, pp. 4157-4170, Aug. 2019.

[22] J. Chen, Y.-C. Liang, Y. Pei, and H. Guo, "Intelligent reflecting surface: A programmable wireless environment for physical layer security," *IEEE Access*, vol. 7, pp. 82599-82612, June 2019.

[23] H. Shen, W. Xu, S. Gong, Z. He, and C. Zhao, "Secrecy rate maximization for intelligent reflecting surface assisted multi-antenna communications," *IEEE Commun. Lett.*, vol. 23, no. 9, pp. 1488-1492, Sept. 2019.

[24] M. Cui, G. Zhang, and R. Zhang, "Secure wireless communication via intelligent reflecting surface," *IEEE Wireless Commun. Lett.*, vol. 8, no. 5, pp. 1410-1414, Oct. 2019.

[25] E. Björnson, Ö. Özdogan, and E. G. Larsson, "Intelligent reflecting surface vs. decode-and-forward: How large surfaces are needed to beat relaying?" *IEEE Wireless Commun. Lett.*, to appear.

[26] M.-A. Badiu and J. P. Coon, "Communication through a large reflecting surface with phase errors," *IEEE Wireless Commun. Lett.*, to appear.

[27] W. Tang, M. Z. Chen, X. Chen, J. Y. Dai, Y. Han, M. D. Renzo, Y. Zeng, S. Jin, Q. Cheng, and T. J. Cui, "Wireless communications with reconfigurable intelligent surface: Path loss modeling and experimental measurement," Nov. 2019. [Online]. Avaliable: https://arXiv.org/abs/1911.05326

[28] Ö. Özdogan, E. Björnson, and E. G. Larsson, "Intelligent reflecting surfaces: Physics, propagation, and pathloss modeling," Oct. 2019. [Online]. Avaliable: https://arXiv.org/abs/1911.03359

[29] C. Masouros and G. Zheng, "Exploiting known interference as green signal power for downlink beamforming optimization," *IEEE Trans. Signal Process.*, vol. 63, no. 14, pp. 3628-3640, July 2015.

[30] M. Alodeh, S. Chatzinotas, and B. Ottersten, "Constructive multiuser interference in symbol level precoding for the MISO downlink channel," *IEEE Trans. Signal Process.*, vol. 63, no. 9, pp. 2239-2252, May 2015.

[31] M. Alodeh, *et al.*, "Symbol-level and multicast precoding for multiuser multiantenna downlink: A state-of-art, classification, and challenges," *IEEE Commun. Surveys Tutorials*, vol. 20, no. 3, pp. 1733-1757, May 2018.

[32] A. Li and C. Masouros, "Interference exploitation precoding made practical: Optimal closed-form solutions for PSK modulations," *IEEE Trans. Wireless Commun.*, vol. 17, no. 11, pp. 7661-7676, Nov. 2018.

[33] Q.-U.-A. Nadeem, A. Kammoun, A. Chaaban, M. Debbah, and M.-S. Alouini, "Intelligent reflecting surface assisted multi-user MISO communication," June 2019. [Online]. Avaliable: https://arXiv.org/abs/1906.02360

[34] S. Khan and S. Y. Shin, "Deep-learning-aided detection for reconfigurable intelligent surfaces," Oct. 2019. [Online]. Avaliable: https://arXiv.org/abs/1910.09136

[35] Z. Wang, L. Liu, and S. Cui, "Channel estimation for intelligent reflecting surface assisted multiuser communications," Nov. 2019. [Online]. Avaliable: https://arXiv.org/abs/1911.03084

[36] A. Ben-Tal and A. Nemirovski, *Lectures on Modern Convex Optimization: Analysis, Algorithms, and Engineering Applications*, Philadelphia, USA: Society for Industrial and Applied Mathematics, 2001.

[37] N. Boumal, B. Mishra, P.-A. Absil, and R. Sepulchre, "Manopt, a MATLAB toolbox for optimization on manifolds," *The J. Mach. Learn. Res.*, vol. 15, no. 1, pp. 1455-1459, 2014.

[38] J. R. Shewchuk, “An introduction to the conjugate gradient method without the agonizing pain,” 1994. [Online]. Available: http://www.cs.cmu.edu/quake-papers/painless-conjugate-gradient.pdf

[39] Z.-Q. Luo, W.-K. Ma, A. M.-C. So, Y. Ye, and S. Zhang, “Semidefinite relaxation of quadratic optimization problems: From its practical deployments and scope of applicability to key theoretical results,” *IEEE Signal Process. Mag.*, vol. 27, no. 3, pp. 20-34, May 2010.